Journal of Alloys and Compounds 509 (2011) 4769–4773

Contents lists available at ScienceDirect

Journal of Alloys and Compounds

journal homepage: www.elsevier.com/locate/jallcom

Enhanced thermoelectric properties of *n*-type Bi_2Te_3-based nanocomposite fabricated by spark plasma sintering

Fei Li[a,b], Xiangyang Huang[a,*], Zhengliang Sun[a,b], Juan Ding[a,b], Jun Jiang[c], Wan Jiang[d], Lidong Chen[a]

[a] CAS Key Laboratory of Materials for Energy Conversion, Shanghai Institute of Ceramics, Chinese Academy of Sciences, 1295 Dingxi Road, Shanghai 200050, China
[b] Graduate University of Chinese Academy of Sciences, 19 Yuquan Road, Beijing 100049, China
[c] Division of Functional Materials and Nano Devices, Ningbo Institute of Material Technology and Engineering, Chinese Academy of Sciences, Ningbo 315201, China
[d] College of Material Science and Engineering, Donghua University, 1882 West Yan-an Road, Shanghai 200051, China

ARTICLE INFO

Article history:
Received 30 September 2010
Received in revised form 19 January 2011
Accepted 20 January 2011
Available online 2 February 2011

Keywords:
Thermoelectric
Al_2O_3
Bi_2Te_3
Nanoparticle

ABSTRACT

Highly dense *n*-type Bi_2Te_3-based thermoelectric materials dispersed with *x* vol.% γ-Al_2O_3 nanoparticles ($x = 0$, 0.4, 1.0, 1.5) were fabricated by spark plasma sintering method. The effects of γ-Al_2O_3 addition on microstructure and the thermoelectric properties were studied. It was found that γ-Al_2O_3 nanoparticles locate both at grain boundaries and inside $Bi_2Se_{0.3}Te_{2.7}$ grains. The nanoparticles induce both potential barrier scattering effect and additional phonon scattering effect, which simultaneously enhance the Seebeck coefficient and reduce the lattice thermal conductivity of the nanocomposites in the measured temperature range of 300–500 K, respectively. The maximum dimensionless figure of merit (ZT_{max}) reaches up to 0.99 for the sample with $x = 1.0$ at 400 K, which is 35% improvement over the Bi_2Te_3-based matrix. More importantly, the average *ZT* value of the sample increases from 0.65 to 0.91 in the temperature range 300–500 K, making the nanocomposites much more applicable in cooling and power generation.

1. Introduction

Recently, considerable interest has been paid in thermoelectric (TE) materials and devices because of their potential applications in the fields of ecology-friendly power generation and solid-state cooling [1]. The efficiency of a material for TE application is determined by the dimensionless figure of merit, defined as $ZT = (S^2\sigma/\kappa)T$, where S, σ, κ and T are the Seebeck coefficient, electrical conductivity, thermal conductivity and absolute temperature, respectively. Therefore, excellent TE materials require a perfect combination of high power factor ($S^2\sigma$) and low thermal conductivity. In order to make a TE device competitive, an average *ZT* of the elements in the application temperature range must be higher than 1.0 in principle [2,3].

Being embodied in the highest *ZT* at room temperature and the production of the commercial module, bismuth telluride (Bi_2Te_3) alloys are currently the best TE materials for practical application. Persistent efforts have been executed to improve *ZT* since the 1950s, especially over the last several years. Great achievements, mainly in p-type Bi_2Te_3-based alloys, have been made by alloying, doping and nanostructuring [4–12]. For example, Poudel et al. synthesized p-type nanostructured BiSbTe bulk alloy by hot pressing nanopowders that were ball-milled from crystalline ingots under inert conditions, and the ZT_{max} value reaches 1.4 at about 373 K [4]. Wang et al. used a one-pot solution process to synthesize colloidal Bi_2Te_3–Te heterogeneous nanostructures (HNs) that comprise Bi_2Te_3 nanoplates and Te nanorods [8]. Unlike p-type Bi_2Te_3-based alloys, the reported ZT_{max} of *n*-type counterpart is still lower than 1.0, limiting the application of Bi_2Te_3-based device.

To enhance the performance of TE materials, one effective way is to reduce the lattice thermal conductivity by incorporating nanoparticles into the matrix on the basis of extra phonon scattering. TiO_2 [13], ZrO_2 [14–16], *etc.* were introduced into filled-skutterudite and half-Heusler TE materials, resulting in a reduction in the lattice thermal conductivity. With respect to Bi_2Te_3-based alloys, Zhao et al. used a simple route involving mechanical alloying and spark plasma sintering (SPS) method to prepare nano-SiC-dispersed Bi_2Te_3-based nanocomposites, which shows reduced thermal conductivity [17]. However, the *ZT* value remains almost unchanged owing to the reason that the incorporation of the SiC nanoparticles deteriorates the electrical conductivity seriously, leading to reduced power factor. This result suggests that SiC is not appropriate candidate as a second nanophase to enhance the TE performance for Bi_2Te_3-based alloys. Therefore, it is necessary to search for suitable nanoparticles to reside in Bi_2Te_3-based alloys. In addition, in order to prepare the nanocomposite with the best performance, we choose the material with optimal stoichiometric, $Bi_2Se_{0.3}Te_{2.7}$, as the matrix.

* Corresponding author. Tel.: +86 21 52412500; fax: +86 21 52413122.
E-mail address: xyhuang@mail.sic.ac.cn (X. Huang).

0925-8388/$ – see front matter © 2011 Elsevier B.V. All rights reserved.
doi:10.1016/j.jallcom.2011.01.155

Table 1
Density and relative density of the sintered samples with different contents of γ-Al_2O_3.

Sample	Density (g/cm^3)	Relative density (%)
$Bi_2Se_{0.3}Te_{2.7}$	7.86	100
$Bi_2Se_{0.3}Te_{2.7}$ + 0.4% Al_2O_3	7.73	98.3
$Bi_2Se_{0.3}Te_{2.7}$ + 1.0% Al_2O_3	7.69	97.8
$Bi_2Se_{0.3}Te_{2.7}$ + 1.5% Al_2O_3	7.59	96.5

In this contribution, we focused on *n*-type Bi_2Te_3-based alloy dispersed with γ-Al_2O_3 nanoparticles. For the sample with different contents of γ-Al_2O_3, the detailed microstructure and TE properties at high temperature were investigated. As will be shown, the incorporation of γ-Al_2O_3 into $Bi_2Se_{0.3}Te_{2.7}$ not only decreases the thermal conductivity, but also enhances the electrical transport properties effectively.

2. Experimental

Based on the method described by Jiang et al. [18], the *n*-type $Bi_2(Te,Se)_3$ alloys were synthesized by zone-melting method. Bi, Te, Se and TeI_4 with purity of 99.9% were used as raw materials. The constituent elements in the proper proportion of $Bi_2Se_{0.3}Te_{2.7}$ were melted at 973 K in a sealed and evacuated quartz tube. The mixture was stirred in the rocking furnace at a certain frequency to ensure the composition homogeneity. The crystal growth was performed with a temperature gradient of 25 K/cm and a growth rate of 0.6 mm/h. The solidified ingot was then crushed into granular powders and sieved into particles about 50 μm with a 200 mesh nylon sieve. Then the powders were mixed with *x* vol.% (*x* = 0, 0.4, 1.0, 1.5) γ-Al_2O_3 particles (about 20 nm) by ball milling, and finally consolidated by the spark plasma sintering equipment (SPS-2040) at 713 K under a pressure of 60 MPa in vacuum for 5 min.

The constituent phases were determined by X-ray diffraction (XRD) (Cu Kα, Rigaku, Rint 2000). The chemical composition of bulk samples was characterized with electron probe microanalysis (EPMA, JEOL, JXA-8100). The microstructure was investigated by transmission electron microscopy (TEM, JEM 2010) with energy dispersive spectrometer (EDS). The electrical conductivity and Seebeck coefficient were measured using commercial equipment (ZEM-3, ULVAC-RIKO) from room temperature to 500 K in helium atmosphere, the shape of the sample is bar-type. The thermal diffusivity (λ) was obtained by laser flash method (Netzsch, LFA427), and converted into thermal conductivity using $k = d\lambda Cp$, where *d* is the density of the sintered sample, and *Cp* is the heat capacity. The density was measured by Archimedes method, and the heat capacity was measured from room temperature to 500 K in argon using a Shimadzu DSC-50.

3. Result and discussion

3.1. Microstructure

Table 1 summarizes the results of density and relative density of the sintered samples with *x* vol.% γ-Al_2O_3 content. It shows that relatively dense sample could be obtained at 713 K under a pressure of 60 MPa. The density decreases with increasing the content of γ-Al_2O_3, indicating that densification retardation occurred for the nanocomposites due to γ-Al_2O_3 dispersion. The inclusion of γ-Al_2O_3 particles in the $Bi_2Se_{0.3}Te_{2.7}$ matrix provides a back stress against the sintering stress during densification, and this effect becomes more remarkable at high Al_2O_3 content [19].

Fig. 1 shows the XRD patterns for the sample with $x = 0$ and $x = 1.0$. All the diffraction peaks for the sample with $x = 1.0$ can be indexed as $Bi_2Se_{0.3}Te_{2.7}$, implying that γ-Al_2O_3 is chemical stable for $Bi_2Se_{0.3}Te_{2.7}$ compound, which is extremely important for the nanocomposite. Since the γ-Al_2O_3 content is very low, the peaks derived from the γ-Al_2O_3 were not found in the XRD patterns. In order to obtain the detailed microstructure of the nanocomposites, the samples were examined by TEM.

Fig. 2(a) shows the TEM image of the γ-Al_2O_3 nanoparticles. It was found that the γ-Al_2O_3 nanoparticles with rod shape has a size of 15–20 nm. There are two kinds of distribution of the γ-Al_2O_3 in the nanocomposites, most of the γ-Al_2O_3 nanoparticles were found to locate at the grain boundaries in the form of aggregation (Fig. 2(b)), this could be also confirmed by the EDS analysis

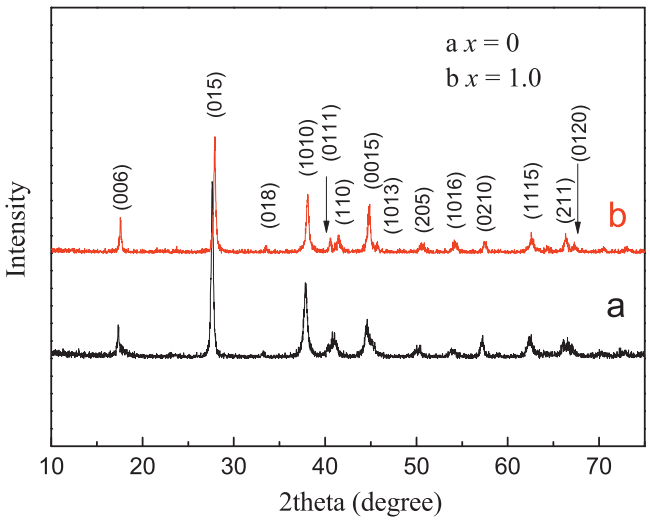

Fig. 1. XRD patterns of the bulk samples: (a) $x = 0$ and (b) $x = 1.0$.

of the grain boundary (Fig. 2(d)). Fig. 2(c) shows that a small quantity of the γ-Al_2O_3 nanoparticles distribute inside the matrix grains with a size of 20 nm. Similar microstructure was also reported for the nanocomposites of $CoSb_3/TiO_2$ [13] and $ZrNiSn/ZrO_2$ [14].

3.2. Electrical transport properties

The temperature dependence of electrical conductivity for all samples between 300 and 500 K is presented in Fig. 3. The electrical conductivity of all samples decreases with increasing temperature, indicating a metallic conducting behavior. Compared to the $Bi_2Se_{0.3}Te_{2.7}$ matrix, the electrical conductivity at a fixed measuring temperature decreases with increasing the γ-Al_2O_3 content. This is mainly attributed to the scattering of the charge carrier due to the introduction of the nanoparticles [20]. The electrical conductivity of the $Bi_2Se_{0.3}Te_{2.7}$ matrix is about 2.0×10^5 S/m at room temperature, which is consistent with reported data in the literature [18]. The sample with $x = 0.4$ shows almost the same electrical conductivity as the matrix in the whole temperature range, while the electrical conductivity for the sample with $x = 1.0$ and $x = 1.5$ is 1.70×10^5 S/m and 1.59×10^5 S/m at room temperature, respectively. It must be pointed out that not only the scattering of the carrier by the nanoparticles but also the lower density lead to the decrease in the electrical conductivity.

The Seebeck coefficient of all samples between 300 and 500 K is plotted in Fig. 4. The negative values of the Seebeck coefficient indicate that all samples are *n*-type semiconductor materials. One can draw an important conclusion that the incorporation of a small amount of the γ-Al_2O_3 nanoparticles notably enhances the Seebeck coefficient of the Bi_2Te_3-based alloys. The maximum value of absolute Seebeck coefficient of $Bi_2Se_{0.3}Te_{2.7}$ matrix is 143 μV/K at around 500 K, which is in good agreement with the data reported in the literature [18]. With the addition of 1.0 vol.% γ-Al_2O_3 nanoparticles, the maximum value of absolute Seebeck coefficient increases to 160 μV/K at 500 K, being 12% enhancement. The increase in the Seebeck coefficient in this nanocomposite could be attributed to the potential barrier scattering [21]. In general, the potential barrier probably formed by localized states resulting from defects such as point defects and dislocations at grain boundaries [22]. The introduction of the γ-Al_2O_3 nanoparticles could bring imperfect structure to the composite system, which would induce more defects at the grain boundaries of $Bi_2Se_{0.3}Te_{2.7}$ and enhance the potential barrier height, and therefore increase the

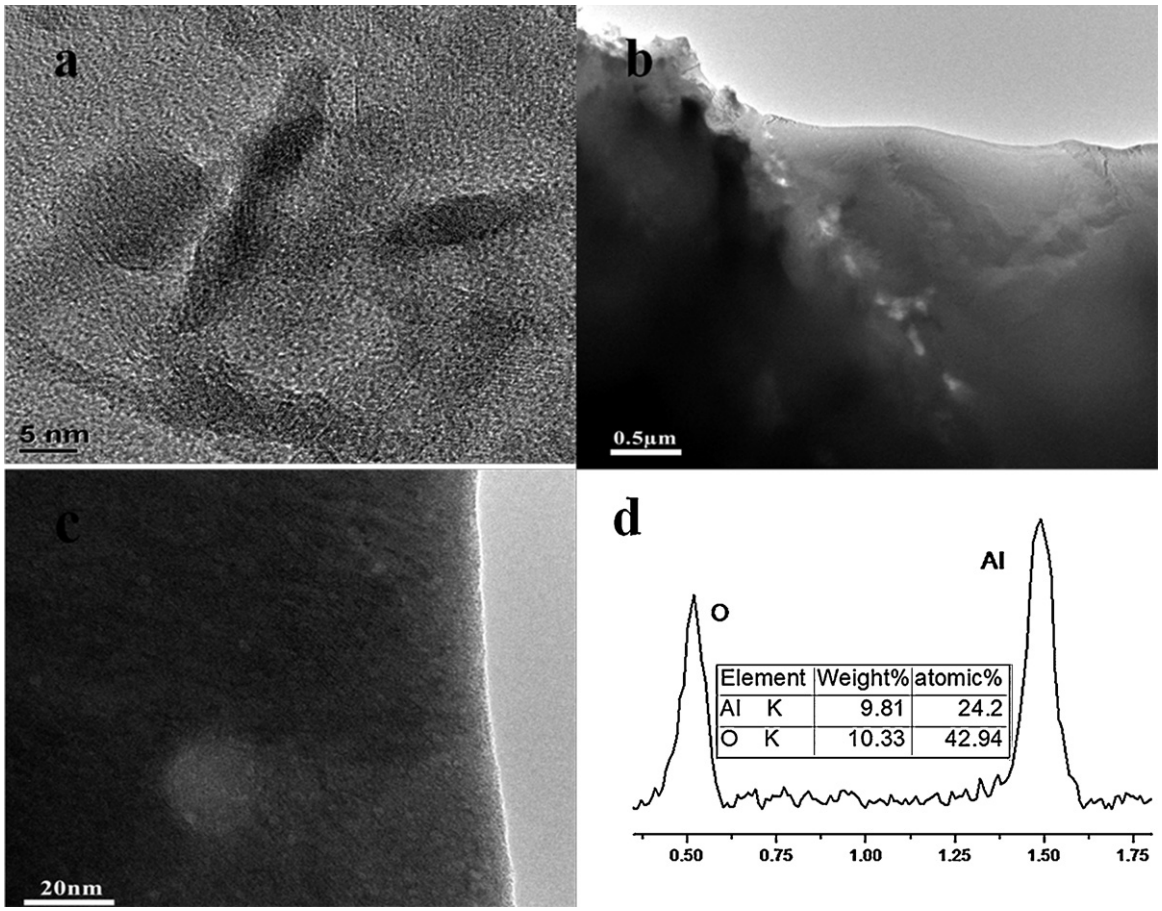

Fig. 2. TEM images of (a) γ-Al_2O_3 nanoparticles; (b) and (c) the bulk sample with $x = 1.0$; and (d) EDS analysis result of the grain boundary in (b).

Seebeck coefficient. Why the sample with $x = 1.5$ show lower absolute Seebeck coefficient than the sample with $x = 1.0$ and $x = 0.4$ is not clear but was duplicated with a second sample. Further research on carrier scattering by the nanoparticles is absolutely needed.

The inset of Fig. 4 is the temperature dependent power factor calculated from the electrical conductivity and Seebeck coefficient. Owing to the increase in the Seebeck coefficient, all nanocomposites show enhanced power factor, indicating that these nanocomposites keep good electrical transport properties. In particular, the power factor of the sample with $x = 0.4$ reaches to $33.7 \times 10^{-4}\,W\,m^{-1}\,K^{-2}$ at room temperature, almost being 50% improvement over the matrix.

3.3. Thermal transport properties

The thermal conductivity as a function of temperature is shown in Fig. 5 and demonstrates clearly that introducing γ-Al_2O_3

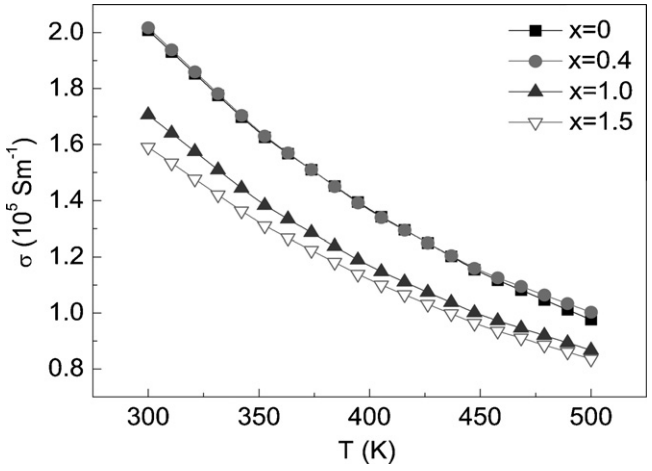

Fig. 3. Temperature dependence of electrical conductivity for $Bi_2Se_{0.3}Te_{2.7}$ + x vol.% γ-Al_2O_3 nanocomposites.

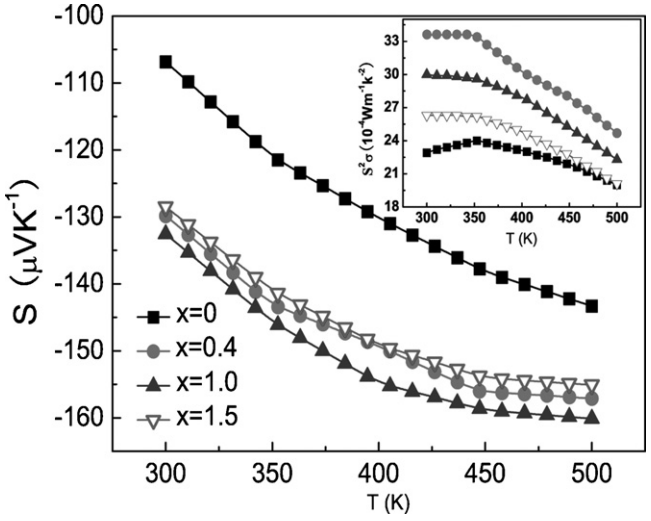

Fig. 4. Temperature dependence of the Seebeck coefficient and power factor (inset) for $Bi_2Se_{0.3}Te_{2.7}$ + x vol.% γ-Al_2O_3 nanocomposites.

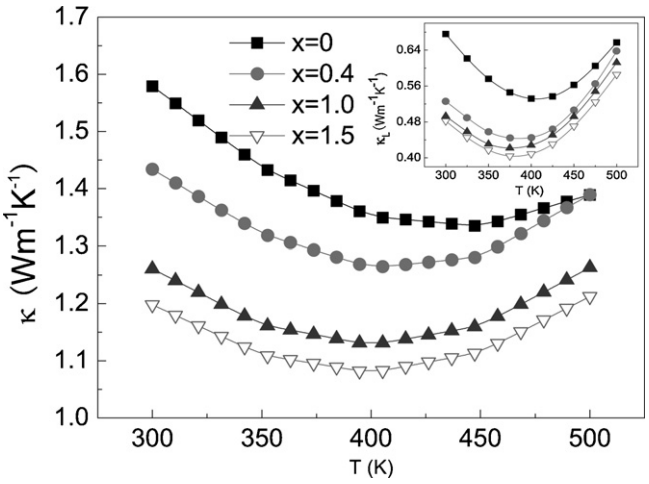

Fig. 5. Temperature dependence of thermal conductivity and lattice thermal conductivity (inset) for $Bi_2Se_{0.3}Te_{2.7}$ + *x* vol.% γ-Al_2O_3 nanocomposites.

nanoparticles into $Bi_2Se_{0.3}Te_{2.7}$ can significantly reduce thermal conductivity in the whole temperature range, at a fixing temperature the sample containing more γ-Al_2O_3 has lower thermal conductivity. The thermal conductivity of $Bi_2Se_{0.3}Te_{2.7}$ is about 1.6 W/m K at 300 K, which is in agreement with the data reported in the literature [18]. The thermal conductivities for the nanocomposites (x = 0.4, 1.0, 1.5) at 300 K are 1.45 W/m K, 1.25 W/m K, 1.2 W/m K, being 10%, 20%, 25% decrease over the matrix, respectively. The total conductivity is a sum of lattice component (κ_L) and electronic component ($\kappa_e = L\sigma T$, L is Lorenz constant). Since the total thermal conductivity is dominated by the electronic contribution in Bi_2Te_3-based compounds [18], and the reduction in electronic thermal conductivity is not notably, especially for the sample with x = 0.4. Accordingly, the depression in thermal conductivity should mainly attribute to the large defects scattering of phonon by the nanoparticle aggregation and additional phonon scattering by the individual nanoparticles inside the matrix [16], namely, the reduction in lattice thermal conductivity (inset of Fig. 5). Compared with the nano-SiC-dispersed composite [17], the present work shows that the nano-γ-Al_2O_3-dispersed composites present larger decrease extent in thermal conductivity, if the content of the nanoparticles is the same. This is probably due to the fact that the γ-Al_2O_3 nanoparticle has smaller size than the SiC nanoparticle. On the other hand, it can be seen from the figure that as increasing temperature the thermal conductivity of all samples first decrease slightly, then increase, which might be attributed to an ambipolar contribution arising from the diffusion of electron–hole pairs with the onset of intrinsic contribution [23].

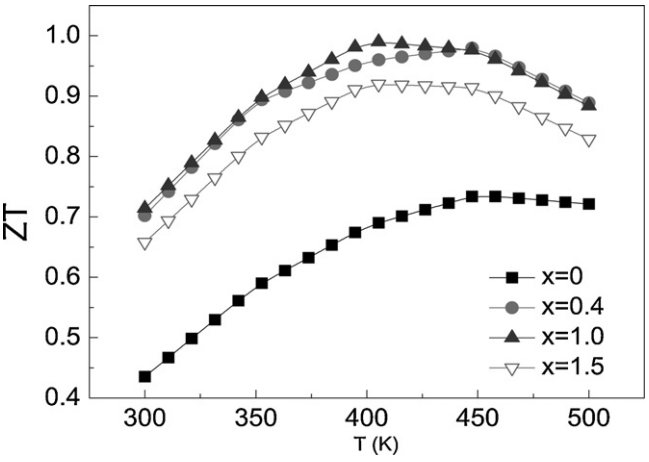

Fig. 6. *ZT* as a function of temperature for $Bi_2Se_{0.3}Te_{2.7}$ + *x* vol.% γ-Al_2O_3 nanocomposites.

3.4. Dimensionless figure of merit ZT

Fig. 6 shows the temperature dependence of the dimensionless figure of merit (*ZT*) for all samples. The sample with x = 1.0 shows the highest *ZT* = 0.99 at about 400 K, approximately an increase of 35% is achieved compared to the γ-Al_2O_3-free sample. More importantly, the average *ZT* value of this sample increase from 0.65 to 0.91 (about 40% improvement) in the temperature range 300–500 K, which makes these materials useful not only for cooling device, but also for power generation effectively.

4. Conclusions

The microstructure and high temperature thermoelectric properties of *n*-type γ-Al_2O_3-dispersed $Bi_2Se_{0.3}Te_{2.7}$ nanocomposites have been studied. It was found that the introduction of the γ-Al_2O_3 nanoparticles to the matrix has an impact on both electrical and thermal transport properties. A large increase of the Seebeck coefficient was observed as a result of potential barrier scattering effect. The nanoparticles scatter not only carrier but also phonons, resulting in the depression in electronic thermal conductivity and lattice thermal conductivity. The optimal content of γ-Al_2O_3 was found to be 1.0 vol.%, and $Bi_2Se_{0.3}Te_{2.7}$–1.0 vol.% γ-Al_2O_3 exhibits the highest *ZT* value of 0.99 at about 400 K, being 35% improvement compared to the matrix. This study suggests that the nanocomposite is also an effective way to further enhance the thermoelectric performance of the Bi_2Te_3-based materials.

Acknowledgements

This work was supported by the National Basic Research Program of China (973 Program) No. 2007CB607505, the National High Technology Research and Development Program of China No. 2007AA03Z233, the National Natural Science Foundation of China No. 50972158, and the National High Technology Research and Development Program of China No. 2009AA03Z210.

References

[1] D.A. Wright, Nature 181 (1958) 834.
[2] D.M. Rowe (Ed.), CRC Handbook of Thermoelectrics, CRC, Boca Raton, FL, 1995.
[3] H.J. Goldsmid, Thermoelectric Refrigeration, Plenum, New York, 1964.
[4] B. Poudel, Q. Hao, Y. Ma, Y.C. Lan, A. Minnich, B. Yu, X. Yan, D.Z. Wang, A. Muto, D. Vashaee, X.Y. Chen, J.M. Liu, M.S. Dresselhaus, G. Chen, Z.F. Ren, Science 320 (2008) 634–638.
[5] Y.Q. Cao, X.B. Zhao, T.J. Zhu, X.B. Zhang, J.P. Tu, Appl. Phys. Lett. 92 (2008).
[6] X.F. Tang, W.J. Xie, H. Li, W.Y. Zhao, Q.J. Zhang, M. Niino, Appl. Phys. Lett. 90 (2007).
[7] Q. Yao, Y.F. Zhou, L.D. Chen, Z.L. Sun, X.H. Chen, J Alloys Compd. 481 (2009) 91–95.
[8] W.S. Wang, J. Goebl, L. He, S. Aloni, Y.X. Hu, L. Zhen, Y.D. Yin, J. Am. Chem. Soc. 132 (2010) 17316–17324.
[9] L.D. Zhao, B.P. Zhang, J.F. Li, H.L. Zhang, W.S. Liu, J. Alloys Compd. 467 (2009) 91–97.
[10] L. Zhou, X.B. Zhang, X.B. Zhao, C.X. Sun, Q. Niu, J. Alloys Compd. 502 (2010) 329–332.
[11] F. Zahid, R. Lake, Appl. Phys. Lett. 97 (2010) 212102.
[12] W.L. Ren, C.X. Cheng, Y.B. Xu, Z.M. Ren, Y.B. Zhong, J. Alloys Compd. 501 (2010) 120–123.
[13] Z. Xiong, X.H. Chen, X.Y. Zhao, S.Q. Bai, X.Y. Huang, L.D. Chen, Solid State Sci. 11 (2009) 1612–1616.
[14] X.Y. Huang, Z. Xu, L.D. Chen, Solid State Commun. 130 (2004) 181.
[15] Z.M. He, C. Stiewe, D. Platzek, G. karpinski, E. Muller, J. Appl. Phys. 101 (2007) 043707.

[16] Z.M. He, C. Stiewe, D. Platzek, G. karpinski, E. Muller, S.H. Li, M. Toprak, M. Muhammed, Nanotechnology 18 (2007) 235602.
[17] L.D. Zhao, B.P. Zhang, J.F. Li, M. Zhou, W.S. Liu, J. Liu, J. Alloys Compd. 455 (2008) 259–264.
[18] J. Jiang, L.D. Chen, S.Q. Bai, Q. Yao, Q. Wang, Mater. Sci. Eng. B 117 (2005) 334–338.
[19] Y. Nakada, T. Kimura, J. Am. Ceram. Soc. 80 (2004) 401.
[20] F. Brochin, B. Lenoir, X. Devaux, R. Martin-Lopez, H. Scherrer, J. Appl. Phys. 88 (2002) 3269.
[21] L.D. Chen, X.Y. Huang, M. Zhou, X. Shi, W.B. Zhang, J. Appl. Phys. 99 (2006) 0064305.
[22] K. Kishimoto, M. Tsukamoto, T. Koyanagi, J. Appl. Phys. 92 (2002) 5331.
[23] H. Muta, T. Kanemitsu, K. Kurosaki, S. Yamanaka, J. Alloys Compd. 469 (2009) 50–55.